Probing mycelium mechanics and taste: The moist and fibrous signature of fungi steak

Thibault Vervenne[a,b,*], Skyler R. St. Pierre[b], Nele Famaey[a], Ellen Kuhl[b,*]

[a]*Department of Mechanical Engineering, KU Leuven, Leuven, Belgium*
[b]*Department of Mechanical Engineering, Stanford University, Stanford, CA, Uuited States*

Abstract

Fungi-based meat is emerging as a promising class of nutritious, sustainable, and minimally processed biomaterials with the potential to complement or replace traditional animal and plant-based meats. However, its mechanical and sensory properties remain largely unknown. Here we characterize the quasi-static and dynamic mechanical behavior of a novel fungi-based steak using multiaxial mechanical testing, rheology, and texture profile analysis. We find that the elastic response under quasi-static compression and shear is isotropic, while the viscous response under dynamic compression is markedly anisotropic, with stiffnesses and peak forces up to four times greater in the cross-plane than in the in-plane direction. Automated model discovery shows that the exponential Demiray model best captures this nonlinear stiffening upon chewing across both directions. These effects are rate-dependent and linked to fluid flow, supporting a poroelastic rather than a purely viscoelastic interpretation. Complementary sensory surveys reveal a strong correlation with mechanical metrics and suggest that we perceive fungi-based steak as more viscous, more moist, and more fibrous than traditional animal- and plant-based meats. Taken together, our findings position fungi-based steak as an attractive, structurally equivalent, and sensorially superior alternative protein source that is healthier for people and for the planet.

Keywords: material characterization, rheology, texture profile analysis, alternative protein, fungi-based meat, mycelium

1. Motivation

The growing global demand for protein creates an urgent need for nutritious and sustainable alternatives to conventional animal meat [32]. Fungi-based proteins from the filamentous mushroom root offer a promising solution [18]. Mycelium is the vegetative lower part of fungi and the largest living organism on earth, that can occupy up to 10 km^2 [7]. Nutritionally, mycelium is low in fat and rich in protein, fibers, and vitamins [2]; it contains all essential amino acids [33]; and it provides health benefits that enhance human immunity, decrease cholesterol levels, and improve the gut microbiome [17]. Structurally, mycelium forms a dense entangled network of branching micro-filaments called hyphae–an assembly of elongated cells, separated by cross walls called septa, all enclosed within the cell wall–resembling the fibrous microstructure of animal meat [11]. Environmentally, mycelium grows rapidly and robustly on low-cost agricultural substrates with minimal land, water, and energy use [23], and generates significantly lower greenhouse gas emissions than traditional animal agriculture [14]. These natural benefits position fungi-based meats as innovative next-generation proteins with the potential to address challenges in both human and planetary health.

Despite this promise, the use of mycelium as a functional biomaterial for food remains poorly understood. The fibrous, filamentous microstructure of mycelium is distinct from both animal and plant tissues [11], and its bulk mechanical properties have not been systematically characterized. While several studies have explored mycelium-based composites for packaging, insulation, and building materials [1], the rheological and textural behavior of edible mycelium-based products remains virtually unstudied. No standardized constitutive model exists for fungi-based meat, and little is known about how its mechanical response varies with the mode of deformation, and with the loading magnitude, rate, and direction. Without this understanding, it is impossible to engineer fungi-based meats that match the mechanical and sensory profiles of traditional animal meat [27].

In this study, we present a comprehensive biomechanical and sensory characterization of a novel fungi-based steak. We perform controlled compression and shear tests in both in-plane and cross-plane directions [26], quantify texture using double-compression texture profile analysis and oscillatory rheology [6], and discover the best fungi steak model and parameters using automated model discovery [15]. To explore to which extent these mechanical features are predictive of our sensory perception, we conduct a sensory survey. We invite sixteen participants to taste and score twelve sensory features, both in-plane and cross-plane, and systematically correlate these features to our mechanical tests. Finally, we compare the performance of the fungi-based steak against eight common commercial meat products [27]. Our overarching question is: *Can fungi-based steak reliably match or exceed the key mechanical and sensory features of traditional animal- and plant-based meats?*

*Corresponding authors
Email address: thibault.vervenne@kuleuven.be, ekuhl@stanford.edu (Ellen Kuhl)

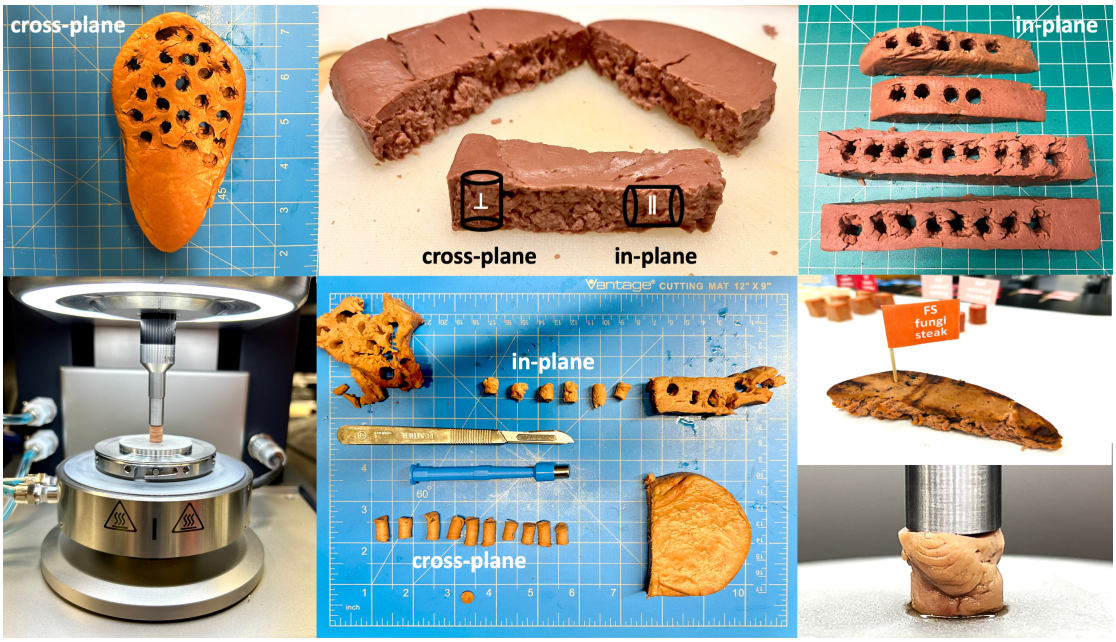

Figure 1: **Sample preparation.** We test fungi-based meat in compression and shear. To prepare the samples, we use a biopsy punch and extract cylindrical samples with 8 mm diameter and 10 mm height, both in-plane and cross-plane. We test a total of $n = 160$ samples, $n = 80$ in each direction, $n = 20$ in quasi-statically in shear and compression, $n = 50$ in uniaxial double compression at five different frequencies, and $n = 10$ in oscillatory shear.

2. Methods

Throughout this study, we test the *fungi-based meat* Mushroom Root Classic Steak (Meati Foods, Boulder, CO) in two orthogonal directions, the *in-plane direction* of the steak parallel to the fiber direction, and the *cross-plane direction* of the steak perpendicular to the fiber direction. According to the ingredient list, the product contains, in descending order by weight, mushroom root (mycelium), and less than 2% of oat fiber, salt, fruit juice for color, vegetable juice for color, natural flavor, and lycopene for color, with mycelium making up 95% of the product. According to the nutrition label, one serving of one steak weighs 120 g and contains 1.5 g or 2% of the percentage daily value of total fat, 9 g or 3% of daily total carbohydrates, with 8 g or 29% of daily dietary fiber, 15 g or 30% of daily protein, and 200 mg or 9% of daily sodium.

We compare the fungi-based meat against three *animal-based meats*, Turkey Polska Kielbasa Sausage (Hillshire Farm, New London, WI), Spam Oven-Roasted Turkey (Spam, Hormel Foods Co, Austin, MN), and Classic Uncured Wieners (Oscar Mayer, Kraft Heinz Co, Chicago, IL), and five *plant-based meats*, Ham-Style Roast Tofurky (Tofurky, Hood River, OR) Vegan Frankfurter Sausage (Field Roast, Seattle, WA), Plant-Based Signature Stadium Hot Dog (Field Roast, Seattle, WA), Organic Tofu Extra Firm (House Foods, Garden Grove, CA), and Organic Firm Tofu (365 by Whole Foods, Austin, TX). We select these eight comparison products from our previous texture profile analysis and rheological tests [6], and our mechanical tests and sensory surveys [27].

2.1. Sample preparation

We use a biopsy punch to extract cylindrical samples of 8 mm diameter and 10 mm height *in-plane*, parallel to the fiber direction, and *cross-plane*, perpendicular to the fiber direction. Figure 1 shows the sample preparation process.

2.2. Sample testing

For each direction, in-plane and cross-plane, we prepare $n = 20$ samples for quasi-static shear and compression testing with ten samples each, $n = 50$ samples for uniaxial double compression testing at five frequencies with ten samples each, and $n = 10$ samples for oscillatory shear testing. We perform all tests using an HR20 discovery hybrid rheometer (TA Instruments, New Castle, DE). Figure 1 displays our compression and shear test setup with the sample mounted in the rheometer. We guaranteed a consistent mounting force below 0.05 N across all samples.

2.2.1. Compression and shear testing for mechanical analysis

For the quasi-static compression tests, we mount the samples and compress them to a stretch of $\lambda = 0.8$ at a stretch rate of $\dot{\lambda} = 0.002$/s, which translates to a total loading time of $t = 100$ s. For the quasi-static shear tests, we mount the samples, fix them at $\lambda = 0.9$ compression, and then shear them to a shear strain of $\gamma = 0.1$ at a shear rate of $\dot{\gamma} = 0.2\%$/s, which translates to a total loading time of $t = 50$ s. Figure 2, top left, illustrates the shear stress-strain and compression stress-stretch behavior, where the curves and the shaded regions represent the mean and standard error of the mean of $n = 10$ tests in the in-plane direction parallel to the fibers in orange and in the cross-plane direction perpendicular to the fibers in brown.

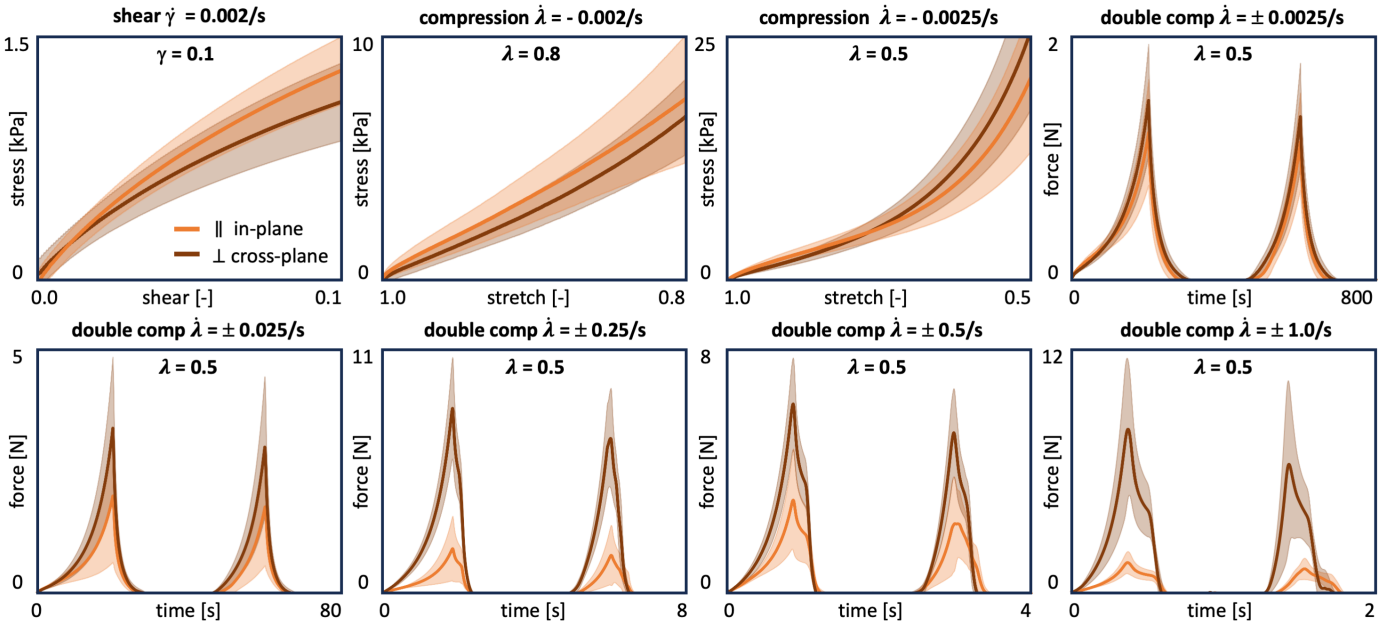

Figure 2: **Shear, compression, and double compression testing.** Quasi-static shear stress-strain data for $\gamma = 0.1$ at $\dot{\gamma} = 0.002$/s for 50 s, quasi-static compression stress-stretch data for $\lambda = 0.2$ at $\dot{\lambda}$ =-0.002/s for 100 s, and $\lambda = 0.5$ at $\dot{\lambda}$ =-0.0025/s for 200 s, and double compression force-time data for $\lambda = 0.5$ at five different rates $\dot{\lambda} = \pm$ 0.0025/s, 0.025/s, 0.25/s, 0.5/s, 1.0/s for 800s, 80s, 8s, 4s, 2s. Curves and shaded regions represent the mean and standard error of the mean of $n = 10$ tests in the in-plane direction in orange and the cross-plane direction in brown.

2.2.2. *Double compression testing for texture profile analysis*

For the double compression tests, we mount the samples, compress them to $\lambda = 0.5$ at a rate $\dot{\lambda}$, unload the samples at the same rate, and repeat this loading and unloading process a second time. We apply five different rates $\dot{\lambda} = \pm$ 0.0025/s, 0.025/s, 0.25/s, 0.5/s, 1.0/s resulting in total test times of 800s, 80s, 8s, 4s, 2s. Figure 2, top right and bottom, illustrates the double compression force-time behavior, where the curves and the shaded regions represent the mean and standard error of the mean of $n = 10$ tests in the in-plane direction parallel to the fibers in orange and in the cross-plane direction perpendicular to the fibers in brown.

2.2.3. *Oscillatory shear testing for rheological analysis*

For the oscillatory shear tests, we mount the samples and fix them at $\lambda = 0.9$ compression, quasi-statically. We first perform an initial amplitude sweep test, oscillating at 0.5 Hz, with shear amplitudes ranging from $\gamma = 0.01\%$ to $\gamma = 60\%$. From the recordings, we determine the shear amplitude within the linear viscoelastic regime for the subsequent frequency sweeps. We then perform frequency sweep tests from $\dot{\gamma} = 0.1$ rad/s to $\dot{\gamma} = 100$ rad/s at $\gamma = 2\%$ shear. From the data < 5 rad/s, We extract the storage modulus G', loss modulus G'', complex shear modulus G^*, and phase angle δ and report the mean and standard error of the mean of $n = 10$ tests in the in-plane and cross-plane directions.

2.3. *Mechanical analysis*

The quasi-static compression and shear tests serve as the basis for the mechanical analysis. To characterize the *non-linear elastic* behavior, we perform automated model discovery to discover the *one-term model* and *two-term model* that best explain the quasi-static behavior throughout 50% compression in the in-plane and cross-plane directions. We use an eight-term constitutive neural network that takes the first and second invariants as input and has two hidden layers with linear and quadratic functions in the first layer and the identity and exponential functions in the second layer [15]. We combine the network with L_1-regularization using a regularization parameter of $\alpha = 0.001$ [19], to reduce the number of terms to either one or two, and discover the best one- and two-term models out of eight and 28 possible models [16]. To characterize the *linear elastic* behavior, we perform a linear regression on the quasi-static compression and shear data throughout 20% compression and 10% shear to extract the compressive, shear, and mean stiffnesses [27]. We postulate a linear stress-strain relation, $\sigma = E \cdot \varepsilon$, and determine the *compressive stiffness*, $E_{\text{com}} = (\boldsymbol{\varepsilon} \cdot \boldsymbol{\sigma})/(\boldsymbol{\varepsilon} \cdot \boldsymbol{\varepsilon})$, from the recorded strain-stress pairs $\{\varepsilon; \sigma\}$ using linear regression. Similarly, we postulate a linear shear stress-strain relation, $\tau = \mu \cdot \gamma$, convert the shear modulus μ into the shear stiffness, $E_{\text{shr}} = 2\,[\,1 + \nu\,]\,\mu = 3\,\mu$, and determine the *shear stiffness*, $E_{\text{shr}} = 3\,(\boldsymbol{\gamma} \cdot \hat{\boldsymbol{\tau}})/(\boldsymbol{\gamma} \cdot \boldsymbol{\gamma})$, from the recorded shear strain-stress pairs $\{\gamma; \tau\}$. Finally, we average the stiffnesses in compression and shear to obtain the *mean stiffness*, $E_{\text{mean}} = (E_{\text{com}} + E_{\text{shr}})/2$.

2.4. *Texture profile analysis*

The double compression tests serve as the basis for the texture profile analysis. Figure 2, top right and bottom, illustrates the load profile of the double compression test, which consists of two consecutive cycles of 50% compression. Figure 3 shows snapshots of the the unloaded and maximally loaded samples

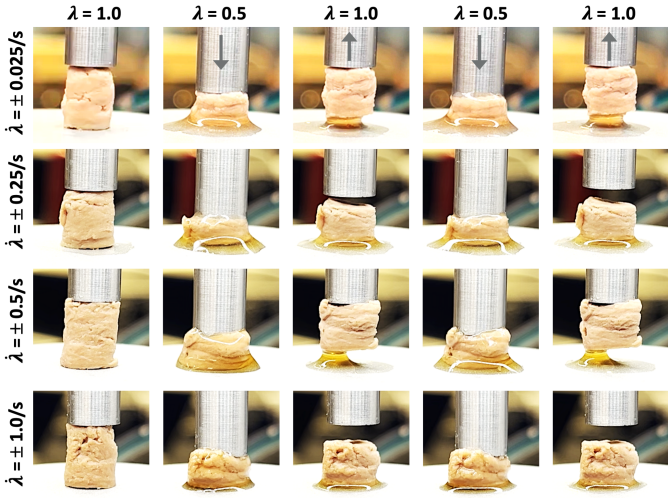

Figure 3: **Texture profile analysis.** Snapshots of the double compression test showing the unloaded and maximally loaded samples at λ = 1.0, 0.5, 1.0, 0.5, 1.0 for four different loading rates, $\dot{\lambda}$ = ± 0.025/s, 0.25/s, 0.5/s, 1.0/s, and a total loading time of 80s, 8s, 4s, 2s. The faster the loading, from top to bottom, the less fluid is squeezed out of the sample during the loading process.

for four different loading rates $\dot{\lambda} = \pm$ 0.025/s, 0.25/s, 0.5/s, 1.0/s. According to standard definitions [3, 9], we denote the peak forces of the first and second loading cycles as F_1 and F_2, the associated loading times as t_1 and t_2, the areas under their loading paths as A_1 and A_3, and the areas under their unloading paths as A_2 and A_4 [6]. We convert the curves into stress vs. strain curves, where the stress $\sigma = F/A$ is the recorded force F divided by the specimen cross section area $A = \pi r^2 = 50.3\,\mathrm{mm}^2$ with $r = 4\,\mathrm{mm}$, and the strain $\varepsilon = \dot{\lambda} t$ is the applied strain rate multiplied by the time t [28]. From the peak force of the first loading cycle F_1, we calculate the peak stress $\sigma_1 = F_1/A$ at peak strain $\varepsilon = -50\%$. From these characteristic values, we extract six texture profile analysis parameters [21]: The *stiffness* $E = \sigma/\varepsilon$ refers to the slope of the stress-strain curve during first compression, when the specimen is compressed to half of its height. The *hardness* F_1 is associated with the peak force during this first compression cycle. The *cohesiveness* $(A_3 + A_4)/(A_1 + A_2)$ characterizes the material integrity during the second loading and unloading cycle, compared to the first cycle, where a value of one relates to a perfectly intact material, whereas a value of zero relates to complete disintegration. The *springiness* t_2/t_1 is associated with recovery and viscosity and describes the speed by which the material springs back to its original state after the second cycle compared to the first. The *resilience* A_2/A_1 is a measure of how well a sample recovers during first unloading path relative to the first loading, where a value of one relates to perfect elasticity whereas a value larger than one indicates plasticity. The *chewiness* $F_1\,(A_3+A_4)/(A_1+A_2)\,t_2/t_1$, the product of hardness, cohesiveness, and springiness, relates to the resistance of a material during the chewing process, with higher chewiness values indicating that the material is more difficult to chew.

2.5. Rheological analysis

The oscillatory shear tests serve as the basis for the rheological analysis. From the amplitude and frequency sweeps, we extract four rheological parameters [6]: The *storage modulus* $G' = G^* \cos(\delta)$ is the elastic modulus, stiffness, or Young's modulus that describes the elastic energy stored in the material during deformation. The *loss modulus* $G'' = G^* \sin(\delta)$ is the viscous modulus that describes the viscous energy dissipated during deformation. The *complex shear modulus* $G^* = G' + i\,G''$ is the sum of the storage and loss moduli and describes the total resistance to deformation as the material is repeatedly sheared. The *phase angle* $\delta = \tan^{-1}(G''/G')$ defines the time lag between the applied shear stress and resulting shear strain and varies between $0° \leq \delta \leq 90°$ where 0° represents a purely elastic and 90° a purely viscous behavior.

2.6. Sensory survey

For the sensory survey, we heat the plain fungi-based steaks, without spices or condiments, and prepare bite-sized samples. We recruit $n = 16$ participants to participate in the Food Texture Survey [27]. We instruct all participants to eat samples of the product product and rank its texture features on a 5-point Likert scale with twelve questions. Each question starts with "this food is ...", followed by one of the following features [22, 30]: *soft*, *hard*, *brittle*, *chewy*, *gummy*, *viscous*, *springy*, *sticky*, *fibrous*, *fatty*, *moist*, and *meaty*. The scale ranges from 5 for strongly agree to 1 for strongly disagree. The participants first eat and rank the steak samples in the cross-plane direction, with the fiber direction perpendicular to the chewing direction, and then in the in-plane direction, with the fiber direction parallel to the chewing direction. This research was reviewed and approved by the Institutional Review Board at Stanford University under the protocol IRB-75418.

2.7. Statistical analysis

We acquire all data using the TRIOS software and analyze the data sets in Python 3.9. To quantify to which extent the in-plane and cross-plane features differ from each other, we perform a Welch's t-test for all texture profile analysis, rheological, and sensory features. In the specific texture profile analysis cases of cohesiveness, springiness and resilience, we use a Mann-Whitney U test based on non-continuous data. We report correlations between texture profile analysis features and loading rate using the Spearman and Pearson correlations coefficients ρ and r, and correlations between rankings of texture profile analysis and sensory survey features using Kendall's rank correlation coefficient τ.

3. Results

Table 1 provides the detailed information of the product, the Mushroom Root Classic Steak, its brand, ingredients, and nutrition facts. The table also summarizes the discovered one- and two-term models, with their parameters and goodness of fit, and the stiffness features, texture profile analysis features, rheological features, and sensory features. All features are reported in

the in-plane and cross-plane directions, with their means and standard deviations. In the following, we compare all features of the fungi-based steak in-plane (FS$^{\parallel}$) and cross-plane (FS$^{\perp}$) against three animal-based products, animal turkey (AT), animal sausage (AS), and animal hotdog (AH), and against five plant-based products, plant turkey (PT), plant sausage (PS), plant hotdog (PH), extrafirm tofu (ET), and firm tofu (FT) [27].

Table 1: **Mushroom Root Classic Steak.** Product; brand; ingredients; nutrition facts; discovered one- and two-term models, parameters, and goodness of fit; stiffness features; texture profile analysis features; rheological features; sensory features. All features are reported in in-plane and cross-plane directions with means and standard deviations.

	in-plane $\parallel$	**cross-plane** $\perp$
product	Mushroom Root Classic Steak	
brand	Meati Foods, Boulder, CO	
ingredients	mushroom root (mycelium), less than 2% of: oat fiber salt, fruit juice, vegetable juice, natural flavor, lycopene	
nutrition facts	serving size of one steak à 120 g contains 1.5 g total fat, 9 g carbohydrates, 8 g dietary fiber, 15 g protein, and 200 mg sodium	
one-term model	w_2 = 9.33 kPa w_2^* = 0.24 R^2 = 0.967	w_2 = 7.23 kPa w_2^* = 0.33 R^2 = 0.985
two-term model	w_1 = 2.35 kPa w_2 = 0.64 kPa w_2^* = 0.43 R^2 = 0.972	w_1 = 1.96 kPa w_2 = 0.68 kPa w_2^* = 0.68 R^2 = 0.985
stiffness	E_{com} = 38.7 ± 11.5 kPa E_{shr} = 42.6 ± 7.2 kPa E_{mean} = 40.7 kPa	E_{com} = 33.6 ± 7.3 kPa E_{shr} = 36.8 ± 8.5 kPa E_{mean} = 35.2 kPa
texture profile analysis	stiff 84.86±60.53 kPa hard 2.13±1.52 N cohesive 0.60±0.09 springy 0.45±0.05 resilient 0.38±0.03 chewy 0.67±0.66 N	stiff 350.56±94.56 kPa hard 8.81±2.38 N cohesive 0.70±0.04 springy 0.54±0.06 resilient 0.41±0.03 chewy 3.33±0.90 N
rheology	G' = 36.7 ± 4.5 kPa G'' = 9.2 ± 0.7 kPa G^* = 37.9 ± 13.8 kPa tan(δ) = 0.254 ± 0.016	G' = 25.2 ± 2.9 kPa G'' = 6.3 ± 0.5 kPa G^* = 25.9 ± 7.6 kPa tan(δ) = 0.252 ± 0.018
sensory survey	soft 4.2±0.8 hard 2.1±0.7 brittle 2.2±1.4 chewy 3.9±0.9 gummy 3.3±1.4 viscous 3.4±1.1 springy 2.3±1.2 sticky 3.0±1.0 fibrous 4.3±0.9 fatty 1.9±1.0 moist 3.8±0.9 meaty 3.5±1.2	soft 3.5±0.9 hard 2.5±1.0 brittle 2.3±1.3 chewy 4.6±0.5 gummy 3.9±1.1 viscous 3.6±1.0 springy 2.8±1.3 sticky 3.6±1.3 fibrous 4.3±0.9 fatty 1.9±1.0 moist 4.1±0.5 meaty 3.3±1.3

3.1. Mechanical analysis

Figure 4 summarizes the results of the automated model discovery to characterize the *non-linear elastic* behavior of the fungi-based meat in the in-plane and cross-plane directions for quasi-static compression up to 50%. The dots indicate the experimental data of the $n = 10$ quasi-static compression tests, the dark and light red areas highlight the contributions of the individual model terms, and the R^2 values quantify the goodness of fit. Interestingly, the constitutive neural network discovers the same one-term model for both directions, the exponential *Demiray model* [5], $\psi = w_2\,[\exp(w_2^*\,[I_1 - 3]) - 1]$, with a linear exponential term of the first invariant, $I_1 = \lambda^2 + 2/\lambda$. Figure 4, top row, shows its fit to the mean experimental data with the discovered stiffness-like and nonlinearity parameters $w_2 = 9.33$ kPa and $w_2^* = 0.24$ for the in-plane model and $w_2 = 7.23$ kPa and $w_2^* = 0.33$ for cross-plane model. Similarly, the network also discovers the same two-term model for both directions, the linear *neo Hookean* model [31] combined with the the exponential *Demiray model* [5], $\psi = w_1\,[I_1 - 3] + w_2\,[\exp(w_2^*\,[I_1 - 3]) - 1]$, with linear and linear exponential terms of the first invariant. Figure 4, bottom row, shows its fit to the mean experimental data with the discovered stiffness-like and nonlinearity parameters $w_1 = 2.35$ kPa, $w_2 = 0.64$ kPa, and $w_2^* = 0.43$ for the in-plane model and $w_1 = 1.96$ kPa, $w_2 = 0.68$ kPa, and $w_2^* = 0.68$ for the cross-plane model. From the experimental data and from the dominance of the linear neo Hookean term in the small-stretch regime, we conclude that the stretch-stress behavior or the fungi-based meat can be approximated as linear until a compression level of about 80%. This is why we now simplify the analysis and explore the material behavior assuming a linear material response.

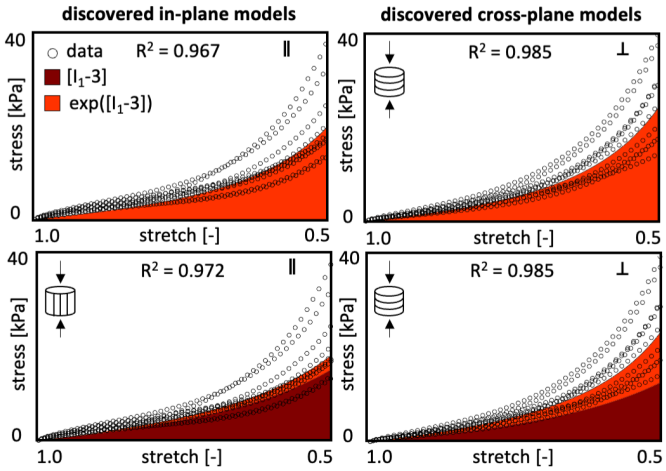

Figure 4: **Mechanical analysis. Automated model discovery.** The constitutive neural network discovers the exponential Demiray model as the best-fit one-term model and a combination of the linear neo Hookean model and the exponential Demiray model as the best-fit two-term model for both the in-plane and cross-plane directions. The dots indicate the experimental data of the $n = 10$ quasi-static compression tests, the dark and light red areas highlight the contributions of the linear and exponential first-invariant terms, the R^2 values quantify the goodness of fit.

Figure 5 summarizes the results of the linear regression to characterize the *linear elastic* behavior of the fungi-based meat in the in-plane and cross-plane directions for quasi-static compression up to 20% and shear up to 10%. The three bar graphs illustrate the in-plane and cross-plane compressive stiffness, shear stiffness, and mean stiffness of the fungi-based steak. All stiffness values are fairly similar, with the stiffnesses in the in-plane direction, $E_{com} = 38.7 \pm 11.5$ kPa, $E_{shr} = 42.6 \pm 7.2$ kPa, and $E_{mean} = 40.7$ kPa being slightly larger than in the cross-plane direction, $E_{com} = 33.6 \pm 7.3$ kPa, $E_{shr} = 36.8 \pm 8.5$ kPa, and $E_{mean} = 35.2$ kPa. For comparison, we also include the values of three animal-based products, animal turkey, animal sausage, and animal hotdog, and five plant-based products, plant turkey, plant sausage, plant hotdog, extrafirm tofu and firm tofu [27]. We observe that plant hotdog with 38.2 kPa, animal sausage with 37.5 kPa, and animal hotdog with 37.1 kPa have similar mean stiffnesses as fungi steak, while plant turkey with 223.7 kPa is about five times as stiff, plant sausage with 103.9 kPa and animal turkey with 71.1 kPa are about twice as stiff, and firm tofu with 26.3 kPa and extrafirm tofu with 24.3 kPa are slightly softer.

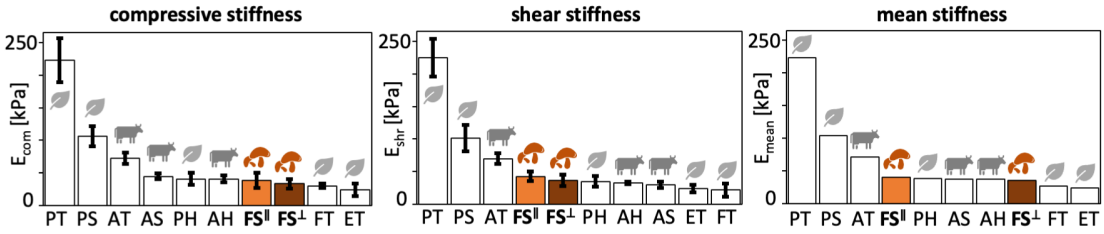

Figure 5: **Mechanical analysis. Compressive stiffness, shear stiffness, and mean stiffness.** In-plane and cross-plane values for fungi-based product, highlighted in orange and brown, compared to animal- and plant-based products. FS$^{\parallel}$ fungi steak in-plane, FS$^{\perp}$ fungi steak cross-plane, AT animal turkey, AS animal sausage, AH animal hotdog, PT plant turkey, PS plant sausage, PH plant hotdog, ET extrafirm tofu, and FTfirm tofu.

3.2. Texture profile analysis

Figure 6 summarizes the results of the double compression test of the fungi-based meat in the in-plane and cross-plane directions for varying loading rates for compression up to 50%. The darkest color highlights the slowest loading rate of $\dot{\lambda} = \pm$

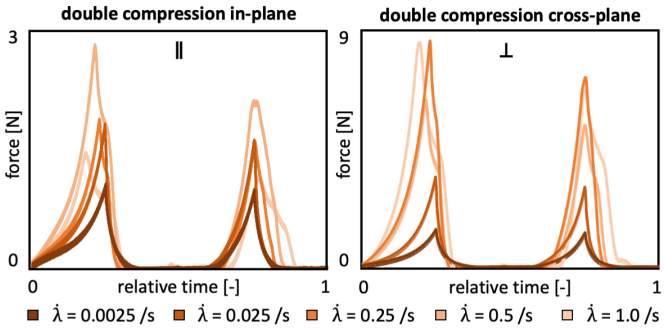

Figure 6: **Texture profile analysis. Loading rate sensitivity of force-time response.** In-plane and cross-plane force-time behavior during the double compression test for five different loading rates, $\dot{\lambda} = \pm$ 0.0025/s, 0.025/s, 0.25/s, 0.5/s, 1.0/s, and a total loading time of 800s, 80s, 8s, 4s, 2s. The faster the loading, from dark to light, the larger the peak force at 50% compression.

0.0025/s for a total experimental time of 800 s and the lightest color highlights the fastest rate of $\dot{\lambda} = \pm$ 1.0/s for a time of 2 s. The curves reflect two general trends: The faster the loading, from dark to light, the larger the peak force at 50% compression. At faster loading rates, the cross-plane peak force is about three times as large as the in-plane peak force, while at slow loading rates, the peak forces are almost identical.

Figure 7 illustrates the six characteristic features of the double compression test of the fungi-based meat in the in-plane and cross-plane directions for varying loading rates for compression up to 50%. The *resilience*, A_2/A_1, a measure of how well the sample recovers during first unloading path relative to the first loading path, displays the strongest correlation to the loading rate $\dot{\lambda}$. Its Spearman correlation coefficients of $\rho = 0.90$ ($p = 0.037$) in-plane and $\rho = 0.90$ ($p = 0.037$) cross-plane indicate a strong, statistically significant, monotonic correlation, and its Pearson correlation coefficients of $r = 0.996$ ($p = 0.00031$) in-plane and $r = 0.996$ ($p = 0.00052$) cross-plane suggest an extremely strong, statistically significant, linear correlation. The *stiffness*, $E = \sigma/\varepsilon$, the slope of the stress-strain curve during the first compression, and the *hardness*, F_1, the peak force during this first compression cycle, only display correlations to the loading rate $\dot{\lambda}$ cross-plane, but not in-plane. Cross-plane, its Spearman correlation coefficient of $\rho = 0.90$ ($p = 0.037$) indicates a strong, statistically significant, monotonic relationship and its Pearson correlation coefficient of $r = 0.76$ ($p = 0.13$) suggests a linear, but not statistically significant trend. Similarly, the *springiness*, t_2/t_1, the relative time by which the sample recovers, only displays correlations to the loading rate $\dot{\lambda}$ cross-plane, but not in-plane. Cross-plane, its Spearman correlation coefficient of $\rho = -0.90$ ($p = 0.037$) indicates a strong, statistically significant, negative monotonic correlation and its Pearson correlation coefficient of $r = -0.944$ ($p = 0.0159$) suggests a strong, statistically significant, negative linear correlation cross-plane. The *cohesiveness*, $(A_3 + A_4)/(A_1 + A_2)$, the material integrity during the second cycle, compared to the first cycle, and the *chewiness*, $F_1\,(A_3 + A_4)/(A_1 + A_2)\,t_2/t_1$, the product of hardness, cohesiveness, and springiness, do not display a statistically significant correlation or general trend with changing loading rates $\dot{\lambda}$. In the following, we focus on the moderate loading rate of $\dot{\lambda} = \pm$ 0.25/s, with a total time of 8 s for two complete chewing cycles.

Figure 8 summarizes the results of the texture profile analysis of the fungi-based meat in the in-plane and cross-plane directions for a double compression to 50% at a loading rate of $\dot{\lambda} = \pm$ 0.25/s. The six bar graphs illustrate the in-plane and cross-plane stiffness, hardness, cohesiveness, springiness, resilience, and chewiness of the fungi-based steak, corresponding to the bright orange bars in Figure 7. Interestingly, for all six features, the cross-plane values are markedly larger than the in-plane values, with statistically significant differences for all features except for resilience. Most notable, the off-plane and in-plane *stiffness* $E = 350.56 \pm 94.56$ kPa and $E = 84.86 \pm 60.53$ kPa and the the off-plane and in-plane *hardness* $F_1 = 8.81 \pm 2.38$ N and $F_1 = 2.13 \pm 1.52$ N vary by more than a factor four, a difference that naturally carries over to the *chewiness* of 3.33 ± 0.90 N and 0.67 ± 0.66 N. At the same time, the *cohesiveness* of 0.70 ± 0.04 and 0.60 ± 0.09, the *springiness* of 0.54 ± 0.06 and 0.45 ± 0.05, the *resilience* of 0.41 ± 0.03 and 0.38 ± 0.03 display only small variations in the off-plane and in-plane directions. Strikingly, the stiffness, hardness, cohesiveness, and chewiness of our fungi-based product all lie within the range of our animal- and plant-based products [6], while its springiness and resilience are significantly smaller both in-plane and cross-plane.

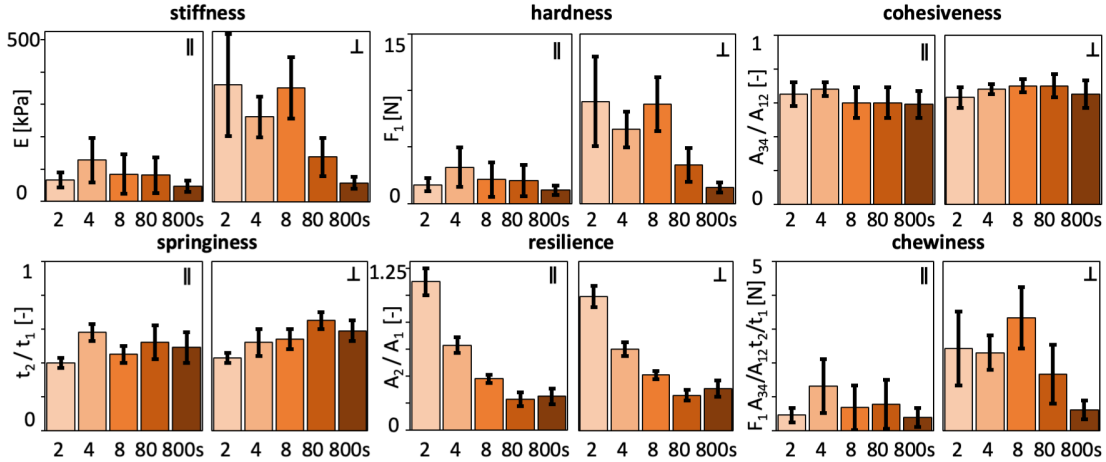

Figure 7: **Texture profile analysis. Loading rate sensitivity of six characteristic features.** In-plane and cross-plane stiffness, hardness, cohesiveness, springiness, resilience, and chewiness for five different loading rates, $\dot{\lambda} = \pm$ 0.0025/s, 0.025/s, 0.25/s, 0.5/s, 1.0/s, and a total loading time of 800s, 80s, 8s, 4s, 2s. The faster the loading, from dark to light, the larger the stiffness, hardness, and the resilience, and the smaller the springiness.

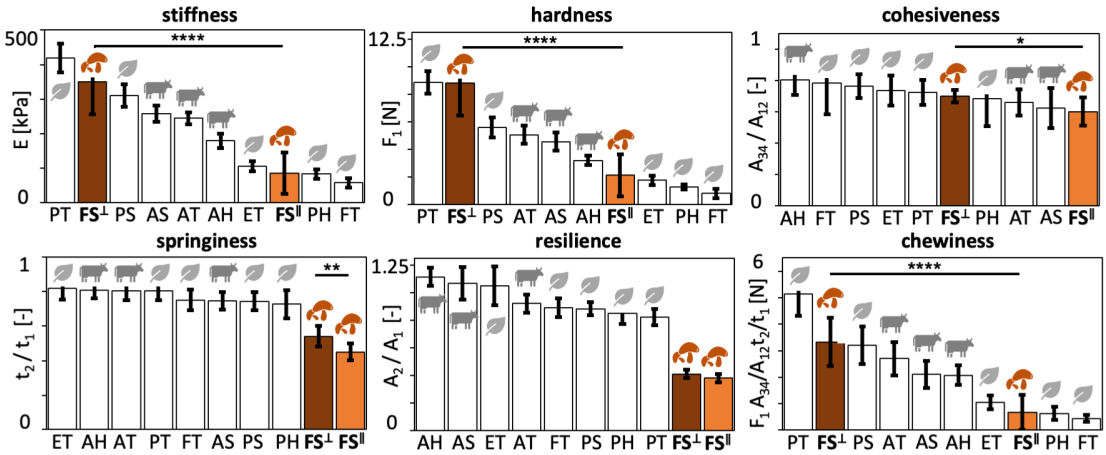

Figure 8: **Texture profile analysis. Stiffness, hardness, cohesiveness, springiness, resilience, and chewiness.** In-plane and cross-plane values at a loading rate $\dot{\lambda} = \pm$ 0.25/s, for a total time of 8 s, for fungi-based product, highlighted in orange and brown, compared to animal- and plant-based products. $FS^{\parallel}$ fungi steak in-plane, $FS^{\perp}$ fungi steak cross-plane, AT animal turkey, AS animal sausage, AH animal hotdog, PT plant turkey, PS plant sausage, PH plant hotdog, ET extrafirm tofu, and FT firm tofu. Statistical significance is indicated as * for $p \leq 0.05$, ** for $p \leq 0.01$, and **** for $p \leq 0.0001$.

3.3. Rheological analysis

Figure 9 summarizes the results of the rheological analysis of the fungi-based meat in the in-plane and cross-plane directions. The four bar graphs illustrate the in-plane and cross-plane storage moduli, loss moduli, complex shear moduli, and phase angles, of our fungi-based product compared to the animal- and plant-based products [6]. We recorded in-plane and cross-plane storage moduli of $G' = 36.7 \pm 4.5$ kPa and $G' = 25.2 \pm 2.9$ kPa, loss moduli of $G'' = 9.2 \pm 0.7$ kPa and $G'' = 6.3 \pm 0.5$ kPa, complex shear moduli of $G^* = 37.9 \pm 13.8$ kPa and $G^* = 25.9 \pm 7.6$ kPa, and phase angles of $\tan(\delta) = 0.254 \pm 0.016$ and $\tan(\delta) = 0.252 \pm 0.018$. These results agree with the our mechanical analysis in the *linear* regime in Figure 5, where the stiffness values in-plane direction are slightly larger than in the cross-plane direction. Interestingly, the storage, loss, and complex shear moduli of our fungi-based product all lie well within the range of our animal- and plant-based products, while the phase angles are notably larger suggesting a more viscous, time-sensitive response.

3.4. Sensory survey

Figure 10 summarizes the results of the sensory survey of the fungi-based meat in the in-plane and cross-plane directions. The twelve bar graphs illustrate the in-plane and cross-plane softness, hardness, brittleness, chewiness, gumminess, viscosity, springiness, stickiness, fibrousness, fattiness, moistness, and meatiness of our fungi-based product compared to the animal- and plant-based products [27]. In the comparison of both directions, the cross-plane scores are larger than the in-plane scores in all categories except for softness and meatiness. In the comparison with the animal- and plant-based products, the fungi-based product stands out in several extremes: It scores highest in five of the twelve categories, *chewiness*, *viscosity*, *stickiness*, *fibrousness*, and *moistness* both in-plane and cross-plane. Both directions also score within the top three in *gumminess* and *meatiness*, and within the bottom three in *springiness*.

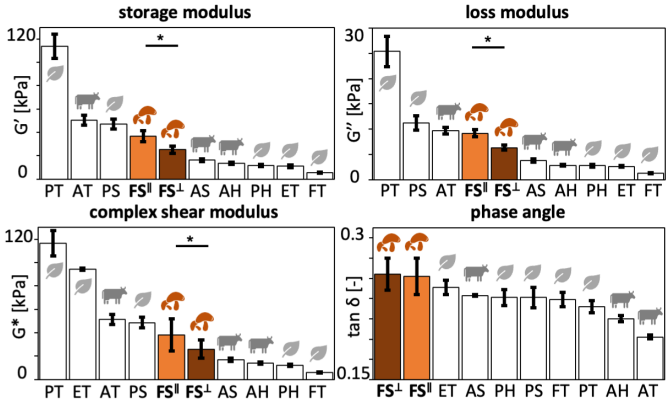

Figure 9: **Rheological analysis. Storage modulus, loss modulus, complex shear modulus, and phase angle.** In-plane and cross-plane values for fungi-based product, highlighted in orange and brown, compared to animal- and plant-based products. $FS^{\parallel}$ fungi steak in-plane, $FS^{\perp}$ fungi steak cross-plane, AT animal turkey, AS animal sausage, AH animal hotdog, PT plant turkey, PS plant sausage, PH plant hotdog, ET extrafirm tofu, and FT firm tofu. Statistical significance is indicated as * for $p \leq 0.05$.

In the remaining four categories, *softness*, *hardness*, *brittleness*, and *fattiness*, the two fungi-based directions score well within the animal- and plant-based products.

Strikingly, the *softness* and *hardness* rankings from our sensory survey in Figure 10 correlate negatively and positively with the *stiffness* and *hardness* rankings from the texture profile analysis in Figure 8. Their Kendall's rank correlation coefficients of $\tau = -0.51$ ($p = 0.047$) for softness and $\tau = +0.51$ ($p = 0.047$) for hardness indicate a statistically significant correlation. The *chewiness* and *springiness* rankings from the sensory survey and the texture profile analysis are only weakly correlated, with $\tau = +0.29$ ($p = 0.293$) for both features, indicating that the correlation is not statistically significant. Finally, the *viscosity* rankings from our sensory survey in Figure 10 and the *phase angle* rankings from our rheological analysis in Figure 9 display a similar trend in rankings, with $\tau = 0.42$ ($p = 0.108$), but the correlation is not statistically significant.

4. Discussion

Texture profile analysis is sensitive to the loading rate. Figure 6 suggests that, the faster the loading, the larger the peak force. Over a range of two orders of magnitude, for loading rates from 0.0025/s to 0.25/s, the in-plane peak force varies by a factor 1.79, from 1.19N to 2.13N, while the cross-plane peak force varies by a factor 6.08, from 1.45N to 8.81N. Figure 7 confirms that faster loading rates result in larger *stiffness*, *hardness*, and *resilience* values, and in smaller *springiness* values. A closer look at the double compression test in Figure 3 provides an explanation for these observations: At slow loading rates, the fluid has enough time to gradually escape the sample. In the extreme case of an infinitely slow loading rate, the machine only probes the solid matrix material. At fast loading rates, the fluid remains trapped in the sample. In the extreme case of an infinitely fast loading rate, the machine probes both the solid matrix and the enclosed fluid. These observations confirm that, especially for visco-elastic food products, the texture profile analysis is highly sensitive to the magnitude of compression λ and to the loading rate $\dot{\lambda}$. To allow for comparisons across different studies and laboratories, these parameters should be standardized or, at a very minimum, be carefully reported and discussed along with the results. For a comparison with previous studies, we recommend a compression level of 50% and a loading rate of 0.25/s [6]. Taken together, we need to be extremely careful when comparing the results of texture profile analyses across different studies with varying magnitudes and rates.

The elasticity of fungi-based steak is isotropic under shear and compression. Figure 2 suggests that the quasi-static response of the fungi-based steak to small shear and compression is almost identical in-plane and cross-plane. Interestingly, the shear response softens with increasing deformation, already at 10% shear, first graph, while the compressive response remains relatively linear, even at 20% compression, second graph. Beyond 25% compression, third graph, we observe a significant stiffening with an interesting cross-over, where the cross-plane behavior shown in brown is initially slightly softer, but then stiffens slightly faster than the in-plane behavior shown in orange. Figure 4 confirms these observations with the same discovered one- and two-term models in both directions. The best one-term model is the Demiray model [5] with a linear exponential first invariant term. The discovered parameters feature a slightly lower initial stiffness cross-plane with $w_2 = 7.23$ kPa compared to in-plane with $w_2 = 9.33$ kPa, but a faster stiffening cross-plane with $w_2^* = 0.33$ than in-plane with $w_2^* = 0.24$. The best two-term model is a combination of the neo Hookean model [31] and the Demiray model [5] with linear and linear exponential first invariant terms. The discovered parameters suggest a dominance of the linear term in-plane with $w_1 = 2.35$ kPa, illustrated through the large dark red area in Figure 4 bottom right, and a an equal contribution of both terms cross-plane with $w_1 = 1.96$ kPa, illustrated through the smaller dark red area in Figure 4 bottom left. Figure 5 confirms that the quasi-static response to small deformations in shear and compression is almost identical in-plane and cross-plane with compressive, shear, and mean stiffnesses varying moderately between 33.6 kPa and 40.7 kPa, all well within the range of the animal- and plant-based comparison products. At first, this observation seems non-intuitive: Many biomaterials are fibrous and anisotropic in nature [16]. We need to keep in mind though that we have only tested in compression and shear. Most biomaterial models deactivate their fiber contributions for compressive loading [13], which agrees with our present observations. We are currently testing the fungi-based steak in tension to explore to which extent its tensile response is truly anisotropic. Taken together, we conclude that under quasi-static shear and compression, the in-plane and cross-plane responses of fungi-based steak are not significantly different, suggesting that, to a first approximation, the elastic behavior of fungi-based steak in shear and compression is isotropic.

The viscosity of fungi-based steak is anisotropic under compression. Figure 2 suggests that the dynamic response of the fungi-based steak to moderate compression is stiffer cross-

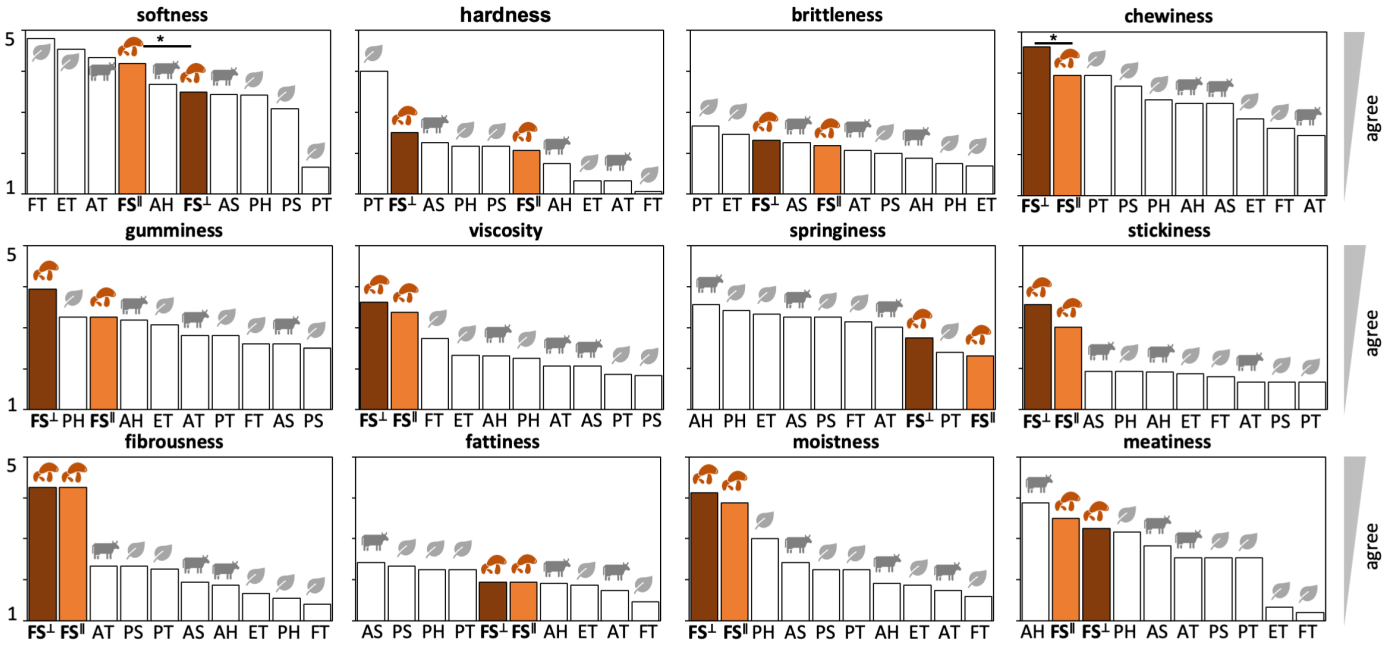

Figure 10: **Sensory survey. Softness, hardness, brittleness, chewiness, gumminess, viscosity, springiness, stickiness, fibrousness, fattiness, moistness, and meatiness.** In-plane and cross-plane values for fungi-based product, highlighted in orange and brown, compared to animal- and plant-based products. FS$^{\parallel}$ fungi steak in-plane, FS$^{\perp}$ fungi steak cross-plane, AT animal turkey, AS animal sausage, AH animal hotdog, PT plant turkey, PS plant sausage, PH plant hotdog, ET extrafirm tofu, and FTfirm tofu. Statistical significance is indicated as * for $p \leq 0.05$.

plane than in-plane. Strikingly, at 50% compression and a loading rate of 0.25/s, the stiffnesses and peak forces of the double compression test vary by a factor four, from 350.56 kPa and 8.81 N cross-plane to 84.86 kPa and 2.13 N in-plane. Figure 8 confirms this observation and shows that, in fact, all cross-plane features of the texture profile analysis are larger than their in-plane counterparts, with statistical significance across all features, stiffness, hardness, cohesiveness, springiness, and chewiness, except for resilience. During the production process, the fungi-based steaks are pressed into shape creating an anisotropic microstructure with a pronounced mycelium orientation in the plane of the steak. We hypothesize that, when loaded in-plane, fluid can escape the sample more easily than when loaded cross-plane. At fast loading rates, this time-dependent viscous effect is dominant, resulting in larger stiffnesses and peak forces cross-plane than in-plane. At slow loading rates, the time-independent elastic effect is dominant, resulting in more isotropic stiffnesses and peak forces. Here we use viscosity as a proxy for the inelastic time-dependent response of the meat products. The large amount of fluid leaving the sample in Figure 3 suggests that, realistically, poroelasticity would be a more appropriate characterization of the constitutive behavior [8]. We are currently performing consolidation-type tests to accurately characterize the poroelastic response in the near future, but will continue to interpret the inelastic time-dependent response as viscoelastic throughout this manuscript. Taken together, we conclude that under dynamic loading, the in-plane and cross-plane responses of fungi-based steak are significantly different, suggesting that the viscous behavior of fungi-based steak is anisotropic.

Our sensory perception agrees with the texture profile analysis. Figure 10 suggests that we perceive fungi-based steak as more *chewy*, more *viscous*, more *sticky*, more *fibrous*, and more *moist* than the animal- and plant-based comparison meats. Strikingly, we also perceive it as more *meaty* than all products, except for animal hotdog. In agreement with the texture profile analysis in Figure 8, we perceive the fungi-based steak as less soft, harder, more springy, and more chewy cross-plane than in-plane. In agreement with the rheological analysis in Figure 9, we perceive the fungi-based steak as more viscous cross-plane than in-plane. Interestingly, our overall softness and hardness rankings from our sensory survey in Figure 10 display a statistically significant correlation with the stiffness and hardness rankings from the texture profile analysis in Figure 8, demonstrating that we can indeed taste stiffness and hardness [27]. Our observations suggest that we can even perceive small textural differences between the in-plane and cross-plane features of fungi-based steak. Most importantly, we perceive pronounced textural differences between fungi-based steak and the eight animal- and plant-based comparison meats. We need to keep in mind though that not only our plant-based products, but also our animal-based products are processed and isotropic [27]. It would be interesting to compare the fungi steak with an animal steak with a similar fibrous and anisotropic microstructural architecture.

Fungi-based steak is a viable alternative to animal- and plant-based meats. Compared to animal-based meat, fungi-based steak is healthier for people and for the planet [18]. It has a *high fiber content*, and is rich in beta-glucans and other prebiotic fibers that have a positive impact on our cholesterol levels

and gut health [17]. It *grows fast* and sustainably, and can be cultivated within days on vertical farms using agricultural waste or low-cost feedstock [10], with *minimal land and water use* [2]. It has a *low environmental footprint*, and produces fewer greenhouse gases than animal agriculture [25]. Compared to plant-based meats, fungi-based steak has a *lean ingredient list* and is not ultra processed. Made up of 95% mushroom root mycelium that grows in a filamentous, fibrous structure [11], it has a *natural meat-like texture*, a *natural umami-type flavor*, and a complete amino acid profile [18]. Its is *minimally processed*, it requires no additives, gums, or binders, it is *allergen-friendly*, and free of soy, gluten, and nuts [12]. A recent study suggests that fungi- and plant-based steaks generally receive a much lower acceptance rate than animal steaks [4]. Our study demonstrates though that fungi-based steaks can comfortably reproduce the mechanical signature of animal- and plant-based meats: Its stiffness and hardness lie well within the range of the comparison meats [6], both in-plane and cross-plane. At the same time, its *high viscosity* and *high moisture* outperform all comparison products. Most notably, with only minimal processing, the fungi-based steak achieves a *more fibrous texture* than all eight comparison products. Our texture profile analysis and our sensory survey both confirm that we can reliably and reproducibly measure and sense significant differences in its in-plane and cross-plane behavior. Strikingly, the fungi-based steak also achieves a *more meaty flavor* than seven of the eight comparison products, which supports the general notion of the umami-type taste and meat-like flavor of mycelium, its main ingredient [18].

5. Conclusion

Fungi-based meats are an emerging class of alternative proteins that offer a nutritious, sustainable, and minimally processed solution to the growing global demand for meat. Our study demonstrates that fungi-based steak–made from 95% of mushroom root mycelium–is a novel, promising, and high-performing alternative to both animal- and plant-based meats: Under quasi-static shear and compression, its elastic response is isotropic. In contrast, under dynamic compression, its viscous response is markedly anisotropic—likely as a result of its high moisture content and inherently fibrous microstructure, with mycelium as the primary component. Our texture profile analysis confirms that the mechanical stiffness, hardness, and resilience of this highly moist product are highly sensitive to both loading magnitude and rate, highlighting the need for standardized testing protocols. Most notably, the mechanical behavior of fungi-based steak lies well within the range of eight commercial animal- and plant-based meats. Strikingly, in some aspects–especially moisture retention and fibrousness–it outperforms all comparison products. Our sensory analysis corroborates these mechanical findings and suggests that fungi-based steak not only mimics a meat-like texture, but also delivers a more umami-rich, meaty flavor than most plant-based alternatives. Taken together, these findings position fungi-based steak as a nutritious, sustainable, and texturally compelling candidate in the future of alternative proteins.

Data Availability

Data and analysis script are freely available at `https://github.com/LivingMatterLab/CANN`.

Acknowledgments

This research was supported by the Research Foundation Flanders FWO through the doctoral fellowship SB1SE2123N to Thibault Vervenne, by the NSF Graduate Research Fellowship, by the Stanford DARE Fellowship, and by seed funding from the Stanford Plant-Based Diet Initiative to Skyler St. Pierre, and by seed funding from Food System Innovations, by the NSF CMMI grant 2320933, and by the ERC Advanced Grant 101141626 to Ellen Kuhl.

References

[1] Alamene, K.K., Anele, J.U., Oke, T.M., Kareem, S.A., Adediran, M., Ajibuwa, O.A. & Anabaranze, Y.O. Mycelium based composites: A review of their bio-fabrication procedures, material properties and potential for green building and construction applications. *Alexandria Engineering Journal* **83** 234–250 (2023).

[2] Amara, A.A. & El-Baky, N.A. Review: Fungi as a source of edible proteins and animal feed. *Journal of Fungi* **9** 73 (2023)

[3] Bourne, M. Texture profile analysis. *Food Technology* **32**, 62-67 (1978).

[4] Cotto, C. Taste of the Industry 2025. A Sensory Analysis of Plant-Based Meats. *NECTAR Food System Innovations* (2025).

[5] Demiray, H. A note on the elasticity of soft biological tissues. *Journal of Biomechanics* **5** 309-311 (1972).

[6] Dunne, R.A., Darwin, E.C., Perez Medina, V.A., Levenston, M.E., St. Pierre, S.R. & Kuhl, E. Texture profile analysis and rheology of plant-based and animal meat. *Food Research International* **205** 115876 (2025).

[7] Ferguson, B.A., Dreisbach, T.A., Parks, C.G., Filip, G.M. & Schmitt, C.L. Coarse-scale population structure of pathogenic *Armillaria* species in a mixed-conifer forest in the Blue Mountains of northeast Oregon. *Canadian Journal of Forest Research* **33** 612-623 (2003).

[8] Franceschini, G., Bigoni, D., Regitnig, P. & G.A. Holzapfel. Brain tissue deforms similarly to filled elastomers and follows consolidation theory *Journal of the Mechanics and Physics of Solids* **54** 2592–2620 (2006).

[9] Friedman H.H., Whitney, J.E. & Szczesniak, A. The texturometer–A new instrument for objective texture measurement. *Journal of Food Science* **28** 390-395 (1963).

[10] Hamza, A., Mylarapu, A., Krishna, K.V. & Kumar, D.S. An insight into the nutritional and medicinal value of edible mushrooms: A natural treasury for human health. *Journal of Biotechnology* **381** 86–99 (2024).

[11] Haneef, M., Ceseracciu, L., Canale, C., Bayer, I.S., Heredia-Guerrero, J.A. & Athanassiou, A. *Scientific Reports* **7** 41292 (2017).

[12] Holt, R.R., Munafo, J.P., Salmen, J., Keen, C.L., Mistry, B.S., Whiteley, J.M., & Schmitz, H.H. Mycelium: A nutrient-dense food to help address world hunger, promote health, and support a regenerative food system. *Journal of Agricultural Food Chemistry* **72** 2697-2707 (2024).

[13] Holzapfel G.A., Gasser T.C. & Ogden R.W. A new constitutive framework for arterial wall mechanics and comparative study of material models. *Journal of Elasticity* **61** 1-48 (2000).

[14] Hong, C., Burney, J.A., Pongratz, J., Nabel, J.E.M.S., Mueller, N.D., Jackson, R.B. & Davis, S. Global and regional drivers of land-use emissions in 1961–2017. *Nature* **589** 554-561 (2021).

[15] Linka, K. & Kuhl E. A new family of Constitutive Artificial Neural Networks towards automated model discovery. *Computer Methods in Applied Mechanics and Engineering* **403** 115731 (2023).

[16] Linka, K. & Kuhl E. Best-in-class modeling: A novel strategy to discover constitutive models for soft matter systems. *Extreme Mechanics Letters* **70** 102181 (2024).

[17] Ma, G., Yang, W., Zhao, L., Pei, F., Fang, D. & Hu, Q. A critical review on the health promoting effects of mushrooms nutraceuticals. *Food Science and Human Wellness* **7** 125–133 (2018).

[18] Maseko, K.H., Regnier, T., Bartels, P. & Meiring, B. Mushroom mycelia as sustainable alternative proteins for the production of hybrid cell-cultured meat: A review *Journal of Food Science* **90** e70060 (2025).

[19] McCulloch, J.A., St. Pierre, S.R., Linka, K. & Kuhl E. On sparse regression, Lp-regularization, and automated model discovery. *International Journal for Numerical Methods in Engineering* **125** e7481 (2024).

[20] Monteiro, C.A., Cannon, G., Levy, R.B., Moubarac, J.C., Louzada, M.L.C., Rauber, F., Khandpur, N. Cediel, G., Neri, D. Martrinez-Steele, E., Baraldi, L.G., Jaime, P.C. Ultra-processed foods: what they are and how to identify them. *Public Health Nutrition* **22** 936-941 (2019).

[21] Nishinari, K., Kohyama, K., Kumagai, H., Funami, T. & Bourne, M. Parameters of texture profile analysis. *Food Science and Technology Research* **19**, 519-521 (2013).

[22] Nishinari, K. & Fang, Y. Perception and measurement of food texture: Solid foods. *Journal of Texture Studies* **49** 160-201 (2018).

[23] Poore, J. & Nemecek, T. Reducing food's environmental impacts through producers and consumers. *Science* **360**, 987–992 (2018).

[24] Rao, M.A. Rheology of Fluid and Semisolid Foods. Principles and Applications. *Food Engineering Series* Springer Science + Business Media, New York (1998).

[25] Souza Filho, P.F., Andersson, D., Ferreira, J.A. & Taherzadeh, M.J. Mycoprotein: environmental impact and health aspects *World Journal of Microbiology and Biotechnology* **35** 147 (2019)

[26] St Pierre, S.R., Rajasekharan, D., Darwin, E.C., Linka, K., Levenston, M.E. & Kuhl E. Discovering the mechanics of artificial and real meat. *Computer Methods in Applied Mechanics and Engineering* **415**, 116236 (2023).

[27] St. Pierre, S.R., Darwin, E.C., Adil, D., Aviles, M.C., Date, A., Dunne, R.A., Lall, Y., Parra Vallecillo, M., Perez Medina, V.A., Linka, K., Levenston, M.E. & Kuhl E. The mechanical and sensory signature of plant-based and animal meat. *Science of Food* **8**, 94 (2024).

[28] St. Pierre, S.R. & Kuhl, E. Mimicking mechanics: A comparison of meat and meat analogs. *Foods* **13** 3495 (2024).

[29] St. Pierre, S.R., Somersille Sibley, L., Tran, S., Tran, V., Darwin, E.C. & Kuhl, E. Biaxial testing and sensory texture evaluation of plant-based and animal deli meat. *bioRxiv* 10.1101/2025.02.19.639170 (2025).

[30] Szczesniak, A.S. Texture is a sensory property. *Food Quality and Preference* **13**, 215-225 (2002).

[31] Treloar, L.R.G. Stresses and birefringence in rubber subjected to general homogeneous strain. *Proceedings of the Physical Society* **60** 135-144 (1948).

[32] van Dijk, M., Morley, T., Rau1, M.L. & Saghai, Y. A meta-analysis of projected global food demand and population at risk of hunger for the period 2010–2050. *Nature Food* **2** 494-501 (2021).

[33] Zhang, X., Zhang, T., Zhao, Y., Jiang, L. & Sui, X. Structural, extraction and safety aspects of novel alternative proteins from different sources. *Food Chemistry* **436** 137712 (2024).